Design and Optimization of Multilayer Cylindrical Magnetic Shield for SERF Atomic Magnetometer Application

Jundi Li, Wei Quan, Bangcheng Han, Zhuo Wang, and Jiancheng Fang

***Abstract*—A set of five-layer cylindrical magnetic shields is designed and constructed to attenuate external geomagnetic field to less than 10 nT (ideally zero). We aim to achieve a shield design having high shielding factor, low magnetic noise, and small volume. However, magnetic noise is incompatible with shielding factor and volume. Thus, there is a compromise. This paper presents an optimization method to acquire a sufficiently effective, low-noise, and lightweight multi-layer shield. The optimization objective and constraints are provided in the form of analytic expressions. The mathematical model is constructed in MATLAB. The optimization is executed in iSIGHT software integrated MATLAB. By optimizing the nonlinear programming quadratic line (NLPQL) algorithm, theoretically the axial shielding factor S^A_{tot} can be increased by a factor of about 390.3, on the premise that the magnetic noise and volume have increased negligibly. Apart from better shielding performance, a combination of optimum parameters is obtained. This optimization method has good universality. As long as certain shielding requirements are determined, the corresponding optimum parameters can be acquired accurately. This method is of great significance for future improvements to shield design.**

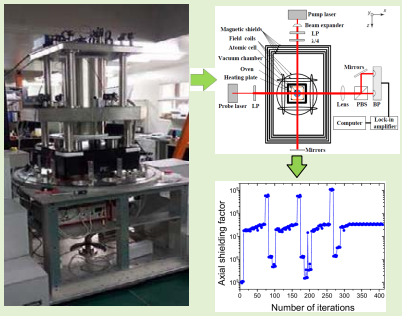

***Index Terms*—Magnetic sensors, design optimization, magnetic shielding, finite element analysis, iterative algorithms.**

I. Introduction

ATOMIC magnetometers operating in spin exchange relaxation free (SERF) demonstrate ultra-high sensitivity on the sub-femtotesla level [1], [2]. Apart from having such high sensitivity, SERF atomic magnetometers are advantageous as they require no cryogenic cooling, have high resolution, and are easy to miniaturize when compared with superconducting quantum interference devices (SQUIDs) [3]. Thus, they may replace SQUIDs in many fields, ranging from fundamental physics experiments to biomagnetism, such as magnetocardiography (MCG), magnetoencephalography (MEG), and magnetic source imaging [4]–[7]. However, to realize the SERF-mode, high atomic number density of alkali metal atoms and extremely weak remanence environment should be achieved simultaneously [8]. The smaller the remanence, the lower the required heating temperature [9]. Therefore, an efficient magnetic shielding system is crucial and urgently required to provide a near-zero magnetic environment.

Magnetic shielding systems are widely applied in various fields, ranging from electronic elements to sophisticated instruments [10], [11], and from fundamental physics research to atomic devices [12]–[15]. The magnetic shielding system mainly includes active magnetic compensation coils and a passive magnetic shield [16]. Passive shielding involves either portable or resident magnetically-shielded rooms [17]–[21]. The performance of resident shielding rooms is excellent; however, they are huge and expensive. Therefore, portable magnetic shielding is often preferred. The shielding performance of the passive shield is mainly evaluated by shielding factors. The higher the shielding factor, the better. Furthermore, magnetic noise caused by the innermost

Manuscript received September 23, 2019; revised October 26, 2019; accepted October 27, 2019. Date of publication October 30, 2019; date of current version January 24, 2020. This work was supported in part by the Beijing Natural Science Foundation under Grant 4191002 and Grant 19D10003, in part by the Key Programs of the National Science Foundation of China under Grant 2016YFB051600, and in part by the National Natural Science Foundation of China under Grant 61773043 and Grant 61721091. The associate editor coordinating the review of this article and approving it for publication was Dr. Yongjia Li. *(Corresponding authors: Wei Quan; Bangcheng Han.)*

The authors are with the Innovative Research Institute of Frontier Science and Technology, Beihang University, Beijing 100191, China, with the Advanced Innovation Center for Biomedical Engineering, Beihang University, Beijing 100191, China, and also with the Beijing Academy of Quantum Information Sciences, Beijing 100094, China (e-mail: quanwei@buaa.edu.cn; hanbangcheng@buaa.edu.cn).

Digital Object Identifier 10.1109/JSEN.2019.2950420

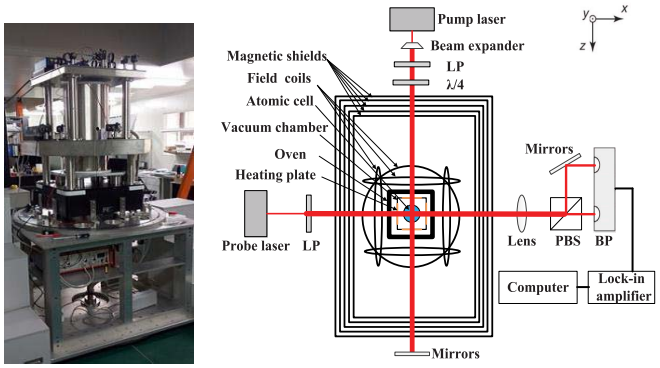

(a) (b)

Fig. 1. Photograph of the five-layer shield and section diagram. (a) Photograph. (b) Cross-sectional drawings.

shielding layer limits further improvements to the sensitivity. Thus, a low-noise MnZn ferrite was utilized by Princeton university as the innermost layer to reduce the magnetic noise generated by the shield itself [22]. Moreover, the influence of magnetic noise can be decreased effectively by optimizing the physical dimensions, such as the aspect ratio of the innermost layer [23]. With the development of the SERF atomic magnetometer, miniaturization becomes critical, especially for the MEG research. Future development is trending towards chip-level atomic magnetometers. Therefore, the volume of the magnetic shield should be as small as possible while maintaining performance.

It is necessary to optimize the shield, but unfortunately, relevant studies are scarce. In 2005, Paperno *et al.* [24] demonstrated that for a double-shell shield, the optimum shell separation should be 5% $\sim$ 10% of the inner shell diameter, which can increase the shielding to 90% of its maximum. Burt and Ekstrom [25] and Paperno *et al.* [26] optimized the shell separation of the magnetic shield for a high axial shielding factor. However, there is no optimization through synthetical consideration, by considering the characteristics of an atomic magnetometer. In this paper, a five-layer shield is designed and optimized to obtain a lightweight high-performance magnetic shield. The optimization is executed by the combination of iSIGHT and MATLAB software. The comparison between the initial and optimal designs is also elaborated. The optimization method is very significant for future design improvements.

II. Shielding Requirements and Principles

A. Shielding Requirements of SERF Magnetometer

Pictures of an atomic magnetometer are shown in Fig.1(a), and its fundamental composition and operation principle is depicted in Fig.1(b). The atomic magnetometer is typically comprised of an atomic cell, oven, no-magnetic electric heating plates, small vacuum chamber, magnetic shielding system, pump and probe optical system, NI DAQ system, etc. The spherical glass cell, with a diameter of 25 mm, is filled with a drop of alkali metal atoms K, several atmospheres of ^{4}He for reducing wall collision relaxation and 60 torr of N_2 gas for quenching. The cell is mounted inside the oven and heated to approximately 200°C by the heating plates. The oven is placed in the vacuum chamber, whose vacuum degree is maintained at approximately 1 $\sim$ 2 mTorr by vacuuming. A five-layer magnetic shield is used to attenuate the external field to less than 10 nT or near zero. Two groups of orthogonal saddle coils along the X and Y axes and a group of Helmholtz coils along the Z axis inside the shield are used to further offset the remanence by applying control fluent. A circularly polarized light is used to polarize atoms, and orthogonal linearly polarized light senses the magnetic field by detecting the optical rotation angle of the linear polarization plane.

The fundamental sensitivity formula for atomic magnetometers is defined as follows.

$$\delta B = \frac{1}{\gamma_e \sqrt{n T_2 V t}} \tag{1}$$

where γ_e is the electron gyromagnetic ratio, n is the atomic number density related to the heating temperature, T_2 is the transverse spin relaxation time, V is the intersection of the pump and probe beam, and t is the measurement time. From the above formula, it can be deduced that when the cell size and heating temperature are both established, only T_2 determines the sensitivity. Therefore, the total spin relaxation rate R_{tot} should be as small as possible. Traditionally, the spin exchange relaxation rate R_{se}^{ee} contributes greatly to R_{tot}; however, it disappears when the spin exchange rate is much larger than the Larmor precession frequency (SERF-mode). At this time, the sensitivity will increase significantly. Moreover, the sensitivity can be characterized by the narrow magnetic resonance linewidth $\Delta\omega$, which is proportional to the amplitude of the residual field inside the cell and is expressed as

$$\Delta\omega = B^2 \left(\frac{g_s \mu_B}{\hbar(2I+1)}\right)^2 \frac{(2I+1)^2\left[q_{lp}^2 - (2I+1)^2\right]}{2R_{SE} q_{lp}^3} \tag{2}$$

where B is the residual magnetic field, g_s and μ_B are the Lade and Boer factors, respectively, I is the nuclear spin, q_{lp} is the slow-down factor operating on low polarization, $\hbar$ is the reduced Planck constant, and R_{SE} is the spin exchange rate. According to (2), the smaller the residual magnetic field is, the narrower the linewidth is and the higher the sensitivity is. In addition to the magnitude of remanence, the existence of the magnetic field gradient ∇B causes resonance linewidth broadening owing to spin gradient relaxation, which will decrease spin precession coherence time and decrease the sensitivity. The mathematical expression for gradient relaxation R_{gr} is as follows:

$$R_{gr} = \gamma \nabla B \tag{3}$$

The cell has a certain volume rather than a point. Therefore, the magnetic field should have a sufficiently large uniform region. The sensitivity of the SERF magnetometer is so high that it is impossible to measure the minimum magnetic field directly. Thus, the sensitivity is not a traditional definition, but rather obtained by the linewidth ΔB divided by the signal-to-noise ratio S/N, $\delta B = \Delta B/(S/N)$ [9]. To acquire such superhigh sensitivity, the detection signal noise from the NI DAQ system and other systems should be extremely low. Presently, the magnetic noise generated by the innermost

shield is the key factor limiting enhancements to the sensitivity. Therefore, the magnetic noise arising from the shield should be sufficiently low.

In summary, the requirements for the multi-layer magnetic shield are as follows. First, to ensure that the atomic magnetometer operates in the SERF regime, the remanence should be less than 10 nT, ideally approaching zero. Second, the remanence gradient should be minimal. Generally, the atomic cell is not a point but has a certain volume (about diameter of 25 mm or less); thus, the homogeneous region inside the shield should be large in the vicinity of the atomic cell under certain uniformity. Third, the magnetic noise generated by the shield should be minimal. Finally, for future miniaturization requirements, the shield volume should be minimal.

B. Shielding Principle

The shielding mechanism depends primarily on the material used. According to the properties of permeability and conductivity, it can be principally divided into two different shielding mechanisms: electromagnetic shielding and magnetic shielding. Further, the magnetic shielding principle includes a flux shunting mechanism and eddy current induced offsetting. The former is typically used in the case of protected areas or apparatus exposed to static and low-frequency magnetic fields, while the latter is used for high frequency AC magnetic fields. The SERF magnetometer herein is mainly exposed to geomagnetic fields; therefore, the shielding principle is the flux shunting.

The shielding factor is associated with the screening material, layer number, and dimension parameters such as innermost layer diameter and length, radial spacing, axial spacing, and thickness [16]. It is defined as the ratio of the external field B_o without the shield to the internal field B_i at the same point.

$$S = B_o/B_i \tag{4}$$

III. Structure and Analysis of Multi-Layer Magnetic Shield

A. Structure of the Magnetic Shield

A five-layer coaxial cylindrical shield with high permeability of permalloy 1J85, rather than a superconducting magnetic material or Metglas [27], is designed and constructed. Fig.2 (a) and Fig.2 (b) present the photograph and section view of the five-layer shield, respectively. The shield is assembled from five single layers and isolated by PEEK plastic interlayers between layers. Each shielding layer is composed of a bucket and an end cover. The assembly has inner diameters ranging from 240 to 330.6 mm and lengths from 586.4 to 677 mm, with different thicknesses in each layer ranging from 1 to 2 mm. The specific parameters of the shield are listed in Table I. There are five openings on the shielding assemblies. Two 25 mm holes in the Z-axis direction are drilled through to provide an optical path for the pumping beam, electric cable paths for the degaussing wire and compensating coils, and access paths for the fluxgate probe. Two holes with diameters of 25 mm in the transverse X-axis direction are used for the probe beam paths whereas one hole with a diameter of 25 mm in transverse Y-axis direction is used for the connecting vacuum line.

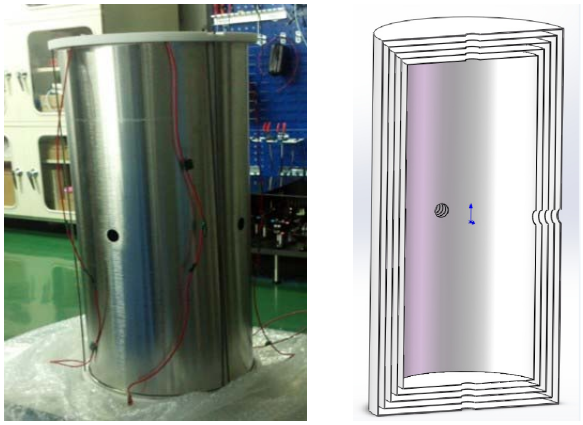

(a) (b)

Fig. 2. Photograph of the five-layer shield and section diagram. (a) Photograph. (b) Cross-sectional drawings.

TABLE I
Design Variables and Initial Values of the Shield

Parameter	Design variable	Initial design
Innermost layer inner diameter	D	240 mm
Innermost layer inner length	L	586.4 mm
Axial gap between layers	G_a	10 mm
Radial gap between layers	G_r	10 mm
First layer thickness	t_1	1 mm
Second layer thickness	t_2	1.3 mm
Third layer thickness	t_3	1.3 mm
Fourth layer thickness	t_4	1.5 mm
Fifth layer thickness	t_5	2 mm

B. Analysis of the Magnetic Shield

The transverse shielding factor formula of a multi-layer concentric finite long shield without openings can be written as follows [28].

$$S_{tot}^T = \prod_{i=1}^{n-1} S_i^T S_n^T \left(1 - \left(\frac{\bar{R}_i}{\bar{R}_{i+1}}\right)^2\right) \tag{5}$$

In Eq.(5), n is the layer number of the magnetic shield. S_i^T and S_n^T are the transverse shielding factor of the i-th and n-th shells, respectively. $\bar{R}_i$ and $\bar{R}_{i+1}$ are the average length of the i-th and $i+1$-th shells. The transverse shielding factor of the i-th layer S_i^T is expressed as

$$S_i^T = \frac{u_i t_i}{2\bar{R}_i} \tag{6}$$

where u_i and t_i are relative permeability and thickness of the i-th layer. The overall axial shielding factor S_{tot}^A is defined as follows [29]

$$S_{tot}^A = \prod_{i=1}^{n-1} S_i^A S_n^A \frac{5}{L_{i+1}/2R_{i+1}} \frac{2R_i + 2R_{i+1} - t_{i+1}}{4L_i + (R_i + R_{i+1} - t_{i+1})} \times \left(1 - \left(\frac{2R_i}{2R_{i+1} - t_{i+1}}\right)^2\right) \frac{f_i}{4N_i} \tag{7}$$

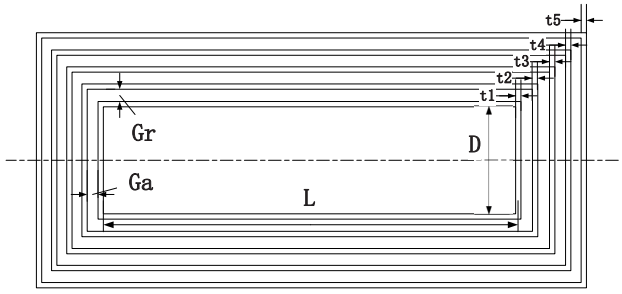

Fig. 3. Parameter variables of cross section of the five-layer cylindrical shield.

In Eq.(7), S_i^A and S_n^A are the transverse shielding factor of the i-th and n-th shells, respectively. $f_i = 1 + L_i/(200R_i)$ is a correction factor due to end cover. The axial shielding factor of the i-th layer S_i^A is as follows

$$S_i^A = (1 + 4N_i S_i^T)/f_i \tag{8}$$

where L_i and R_i are the outer length and radius of the i-th layer, respectively. And $L_i = \bar{L}_i + t_i$ and $R_i = \bar{R}_i + t_i/2$. $\bar{L}_i$ is the average length of the i-th layer. N_i is the demagnetizing factor for a rod [29], [30], as shown below.

$$N_i = -\frac{0.048}{(0.5L_i/R_i)^{0.5}} + \frac{0.329}{0.5L_i/R_i} - \frac{0.053}{(0.5L_i/R_i)^2} \tag{9}$$

The shielding formula without openings is adopted for approximate calculation. This solution is valid when the diameter of the opening is significantly smaller than the shielding size.

C. Relationship Between Performance and Parameters

The geometric parameters of the designed shield are shown in Fig. 3. D and L are assumed to be the internal diameter and length of the innermost shield, respectively. G_r and G_a are the radial and axial clearance between layers, respectively. Thus, the average length $\bar{L}_i$ and radius $\bar{R}_i$ of the i-th layer can be written as follows (i = 1, 2 . . . 5). t_i and t_j are the thicknesses of the i-th and j-th layers, respectively (j = 1, 2, . . . 4).

$$\bar{R}_i = D/2 + (i-1) * G_r + t_i/2 + \sum_{j=1}^{j<i} t_j \tag{10}$$

$$\bar{L}_i = L + 2 * (i-1) * G_a + t_i + 2 * \sum_{j=1}^{j<i} t_j \tag{11}$$

By substituting (10) and (11) into (5)–(9), the transverse shielding factor S_{tot}^T and axial shielding factor S_{tot}^A formulas of the multi-layer shield are functions of the parameters D, L, G_a, G_r, t_1, t_2, t_3, t_4, and t_5.

IV. Optimization of the Magnetic Shield

A. Object Function

Ignoring the opening effect, according to formulas (5) and (7) and the initial design variable values, the computed transverse shielding factor S_{tot}^T and axial shielding factor S_{tot}^A of the five-layer shield are approximately $4.86*10^6$ and $8.25*10^4$. It is observed that the axial shielding factor is far lower than the transverse shielding factor. The axial shielding factor usually limits the sensitivity of atomic magnetometer. Therefore, it should be optimized, and here the axial shielding factor is selected as the main optimization objective.

B. Selection of Design Variables

According to the structure of the multi-layer shield shown in Fig. 3, parameters D, L, G_a, G_r, t_1, t_2, t_3, t_4, and t_5 are selected as optimization variables and their initial values are shown in Table I. The general form of differing thicknesses is considered.

The inner diameter of the innermost layer is inversely proportional to the Johnson magnetic noise. Thus, to reduce the noise, the inner diameter should be as large as possible. However, it is unrealistic to make it excessively large as a high volume would increase costs and would not be conducive to miniaturization in future. Owing to the installation structure, the size of the innermost shield is limited by the outer diameter of the magnetic compensation coil skeleton. How small it can be depends on the size of the inner coil. The homogeneity range of the coils is proportional to the coil size; thus, the coils cannot be too small. The innermost diameter should be set to a reasonable interval. In addition, aspect ratio affects the magnitude of magnetic noise. Considering the magnetic noise, the inner thickness t_1 should be as thin as possible. Once the inner diameter is determined, the inner length and thickness must be selected appropriately to achieve low enough magnetic noise. The spacing between the layers can be set based on experience to ensure high shielding factors. The ranges of the design variables are listed as (unit: mm)

$$\begin{cases} 220 \le D \le 260 \\ 330 \le L \le 560 \\ 2 < G_a < 20 \\ 2 < G_r < 20 \\ 0.05 \le t_1 \le 1 \\ 1 \le t_2, t_3, t_4, t_5 \le 3 \end{cases} \tag{12}$$

C. Constraints

Johnson magnetic noise caused by the innermost shield limits further improvements to the sensitivity of the SERF magnetometer. Therefore, when designing the shield, the noise should be minimized. The Johnson magnetic noise formula is an approximate formula for infinite long cylinders, as shown below.

$$\delta B_{curr} = \frac{\mu_0 \sqrt{kT\sigma t}}{R} \sqrt{\frac{2}{3\pi} G} \tag{13}$$

where $\mu_0 = 4\pi * 10^{-7}\ N/A^2$ is the vacuum permeability, $k = 1.38 * 10^{-23}\ J/K$ is the Boltzmann constant, T is the Kelvin temperature of the magnetic shield, t is the shielding thickness, $R = D/2$ is the radius of the magnetic shield, $\sigma = 1.6*10^6\ \Omega^{-1}*m^{-1}$ is the conductivity of permalloy, G is the parameter related to the ratio of the length to the diameter of the shield L/D, and $G = 0.657$, 0.460, and 0.438 for

TABLE II
PARAMETERS OBTAINED BY OPTIMIZATION TECHNIQUE OF NLPQL

Variables	D	L	G_a	G_r	t_1	t_2	t_3	t_4	t_5
Values (mm)	220	330.7	20	12.6	0.85	2.8	2.5	2.2	1.9

$L/D = 1$, 1.5, and 2, respectively [23]. The contribution of $L/D = 1.5$ and $L/D = 2$ to magnetic noise can be approximately equal, because the noise is only proportional to the square root of G, which is almost equal. Based on (13), the calculated magnetic noise of the designed shield is approximately 8.2 fT/Hz$^{1/2}$. The optimal shield noise should not exceed this value. Based on the dimensional parameters, the entire volume V of the five-layer shield can be expressed in analytical form:

$$V = \sum_{i=1}^{5} V_i \quad (i = 1, 2 \ldots 5) \tag{14}$$

$$V_i = \pi * ((\bar{R}_i + \frac{t_i}{2})^2 * (\bar{L}_i + t_i) - (\bar{R}_i - \frac{t_i}{2})^2 * (\bar{L}_i - t_i)) \tag{15}$$

where V_i is the volume of the i-th layer. According to the formula, the designed shield volume is 0.0053 m^3. The magnetic noise and shield volume are used as constraints. The constraints are summarized as follows:

$$\begin{cases} \delta B_{curr} \leq 8.2 \\ V \leq 0.0053 \\ \bar{L}_i / \bar{R}_i \geq 3 \end{cases} \tag{16}$$

D. Optimization Method and Results

The axial shielding factor S^A_{tot} is the optimization objective. The mathematical representation of the objective is illustrated as follows:

$$max \left\{ S^A_{tot}(D, L, G_a, G_r, t_1, t_2, t_3, t_4, t_5) \right\} \tag{17}$$

Many optimization methods can be considered for multi-layer shield optimization. Here, the NLPQL algorithm is used to identify the precise optimum solution at a certain region of design variables. The analytical formulas of the shielding factors are provided in the front section. The optimization technique is implemented in iSIGHT integrated MATLAB software.

The design parameters obtained by the optimization technique are shown in Table II. Further, the transverse shielding factor S^T_{tot} and axial shielding factor S^A_{tot} calculated with these parameters are approximately 6.65*10^7 and 3.22*10^7, respectively. As shown in Table III, the S^T_{tot} and S^A_{tot} increase by a factor of 390.3 and 13.68, respectively. The optimization curve of the axial shielding factor S^A_{tot} of the five-layer shield is shown in Fig. 4.

The optimization curves and variation tendencies of the design variables are shown in Fig. 5(a)–(i). Compared with the values before optimization, the volume and innermost magnetic noise are relatively unchanged at about 0.0053 m^3 and 8.21 fT/Hz$^{1/2}$, respectively (Table III).

TABLE III
PARAMETERS OBTAINED BY OPTIMIZATION TECHNIQUE OF NLPQL

Design objectives	S^A_{tot}	S^T_{tot}	V	δB_{curr}
Initiate value	8.25*10^4	4.86*10^6	0.0053	8.2
Optimization value	3.22*10^7	6.65*10^7	0.0053	8.21
Increase by a factor	390.3	13.68	1	1.001

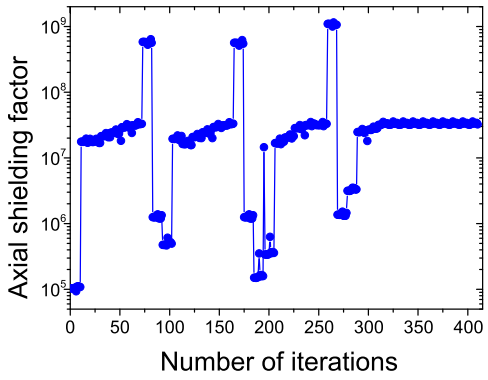

Fig. 4. Optimization curve of the axial shielding factor.

V. FINITE ELEMENT SIMULATION AND EXPERIMENTAL VERIFICATION

The external magnetic field of an atomic magnetometer is its geomagnetic field, the horizontal and vertical components of which are close to 30 uT and 46 uT, respectively. Two standard Helmholtz coils were used to simulate the components using the 2018 version of Ansys Electronics Desktop software. Both coils were 3 m in diameter; however, different currents were passed through them - one was treated to 50,000 mA, and 76,667 mA was applied to the other. The simulation resulted in magnetic fields of 30.0006 uT and 46.001 uT, respectively. The relative errors were less than 0.003%. Conclusively, the finite element method can be effectively applied to simulate the geomagnetic field. Furthermore, four different simplified radial and axial simulation models of the five-layer shield were observed. Fig. 6(a) through Fig. 6(d) illustrate these models without and with openings.

Fig. 7 depicts the corresponding remanence nephogram of a circular region with a diameter of 25 mm. The central remanences in Fig. 7(a) and Fig. 7(b) are approximately 0.0059 nT and 0.0098 nT, respectively. These correspond to the transverse shielding factors of approximately 5.08*10^6 and 3.06*10^6, in cases of without and with openings, respectively. Although there are some deviations from the theoretical calculation (4.86*10^6), the simulation results are still reasonable, because the former adopts an ideal simplified model, and does not consider the influence of assembly clearances between the end cap and the cylinder. On the other hand, the simulation model takes the hole effect into account. The central remanences of Fig. 7(c) and Fig. 7(d) are close to 0.804 nT and 0.921 nT, respectively. These correspond to axial shielding factors of approximately 5.72*10^4 and 4.99*10^4, in case of without and with openings, respectively.

Post optimization, the new, five-layer shield is obtained (Table II). The above outlined simulation is repeated.

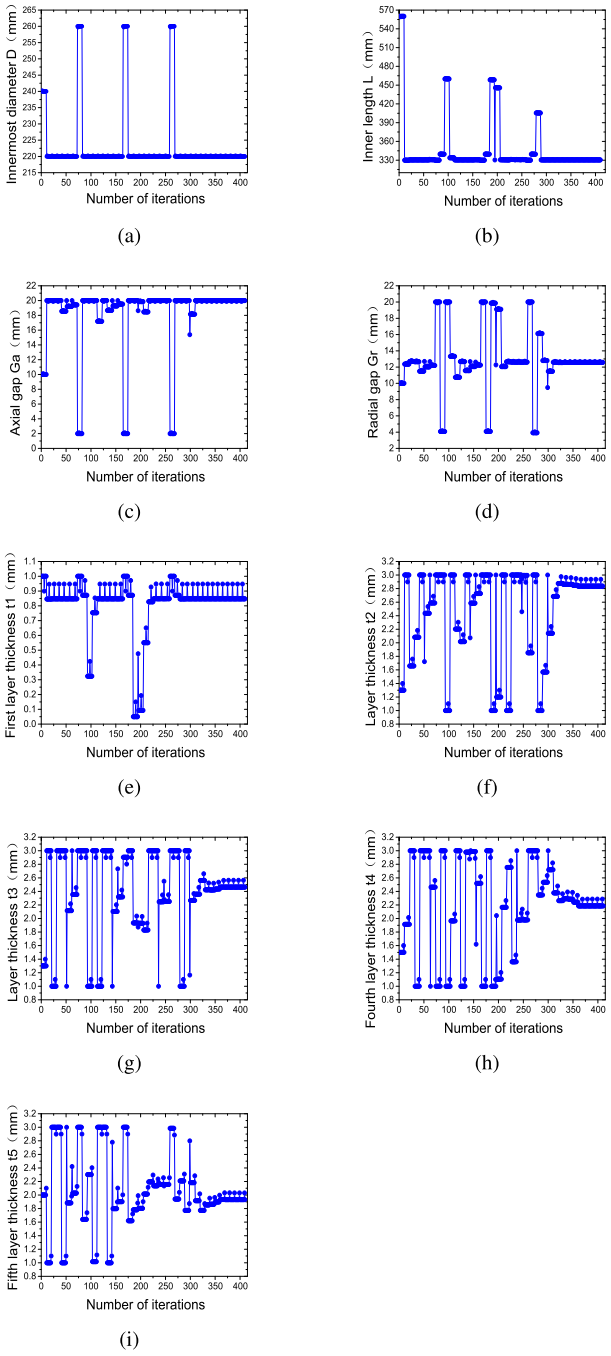

Fig. 5. Optimization curves of design variables including (a) D, (b) L, (c) Ga, (d) Gr, (e) t_1, (f) t_2, (g) t_3, (h) t_4, and (i) t_5.

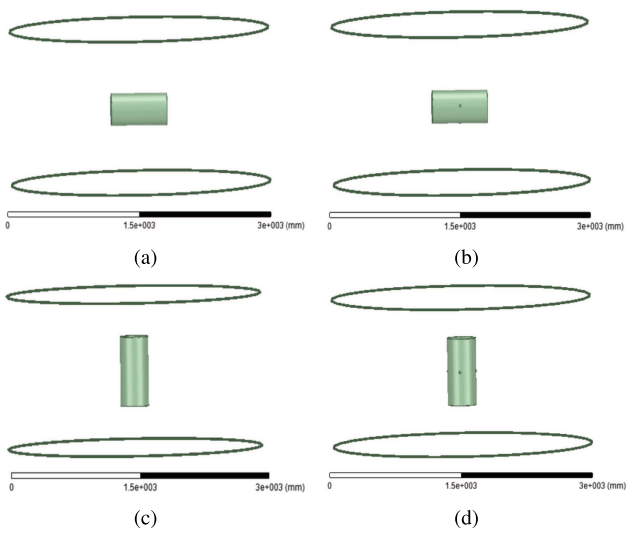

Fig. 6. Four different simplified models of the five-layer shield. (a) Radial simulation model without openings, (b) Radial simulation model with openings, (c) Axial simulation model without openings, (d) Axial simulation model with openings.

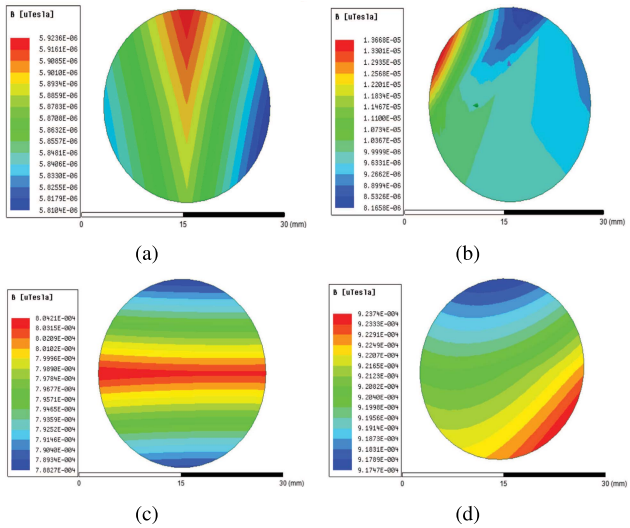

Fig. 7. Corresponding remanence nephogram of a circular region with a diameter of 25 mm. (a) Along the horizontal axis without openings, (b) Along the horizontal axis with openings, (c) Along the vertical axis without openings, (d) Along the vertical axis with openings.

The results demonstrate that the central remanences are approximately 0.003 nT and 0.006 nT, corresponding to the opening transverse and axial shielding factors of approximately $1.0*10^7$ and $7.67*10^6$, respectively. In the new design, the axial shielding factor is higher by nearly two orders of magnitude, in comparison with the original one.

Each shielding layer is made of permalloy 1J85, which is treated by vacuum magnetic annealing in a hydrogen furnace. The relative permeability is assumed to be $2 * 10^4$. Five single-layer shields are assembled first, followed by the measurement of the remanence inside the shields using a CTW-6W fluxgate magnetometer. The difference in measurements in opposite directions is first divided by 2, and the resulting absolute value is considered to eliminate the bias error of the fluxgate. Prior to demagnetization, the transverse and axial central remanences measure ≤ 2 nT. Post degaussing, remanence is remeasured. The remanence distributions in three directions, along the east-west, north-south, and heaven-earth axes are illustrated in Fig. 8(a) through Fig. 8(c). The central remanences in the three directions measure close to 0.05 nT, 0.20 nT, and 0.50 nT, respectively. The corresponding transverse and axial shielding factors are approximately $1.46*10^5$ and $9.2*10^4$, respectively. There are some deviations between the theoretical calculation, simulation, and experimentation, due to several possible reasons, such as incomplete demagnetization, processing technology,

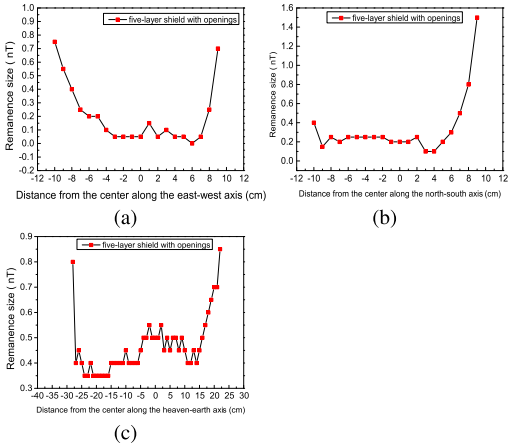

Fig. 8. Remanence distributions in three directions. (a) Along east-west axes, (b) Along north-south axes, (c) Along heaven-earth axes.

assembly and measurement errors, fluxgate bias error, and fluctuation of ambient magnetic field. However, in relative terms, the three methods demonstrate consistency in the trends of different configurations. Therefore, the approximate theoretical formulas can used as an optimization tool.

VI. Conclusion

A designed five-layer cylindrical magnetic shield has been optimized by NLPQL algorithms implemented using ISIGHT software combined with MATLAB. To maximize the axial shielding factor, which is the most critical factor affecting the shielding performance, the axial shielding factor is selected as the optimization objective, while magnetic noise and volume are selected as constraints. The objective and constraints are both provided in the form of analytical expressions. Initial design variables and optimized parameters are presented. After optimization, the axial shielding factor is increased by two orders of magnitude. Moreover, there is no additional increase in the volume and innermost magnetic noise. The proposed approach has good universality for single objective optimization, such as pursuing a smaller volume or lower magnetic noise. The next steps are to optimize the shield with a multi-objective optimization method. According to different target requirements, the scale factor and weight coefficient should be reasonably selected to obtain the optimal multi-layer shield design.

References

[1] H. B. Dang, A. C. Maloof, and M. V. Romalis, "Ultrahigh sensitivity magnetic field and magnetization measurements with an atomic magnetometer," *Appl. Phys. Lett.*, vol. 97, no. 15, Oct. 2010, Art. no. 151110.

[2] I. K. Kominis, T. W. Kornack, J. C. Allred, and M. V. Romalis, "A subfemtotesla multichannel atomic magnetometer," *Nature*, vol. 422, pp. 596–599, Apr. 2003.

[3] K. Kim *et al.*, "Multi-channel atomic magnetometer for magnetoencephalography: A configuration study," *NeuroImage*, vol. 89, pp. 143–151, Apr. 2014.

[4] R. Wyllie, M. Kauer, G. S. Smetana, R. Wakai, and T. G. Walker, "Magnetocardiography with a modular spin-exchange relaxation-free atomic magnetometer array," *Phys. Med. Biol.*, vol. 57, no. 9, p. 2619, 2012.

[5] A. P. Colombo *et al.*, "Four-channel optically pumped atomic magnetometer for magnetoencephalography," *Opt. Express*, vol. 24, no. 14, pp. 15403–15416, 2016.

[6] D. Budker and M. Romalis, "Optical magnetometry," *Nature Phys.*, vol. 3, no. 4, p. 227, Apr. 2007.

[7] I. M. Savukov and M. V. Romalis, "NMR detection with an atomic magnetometer," *Phys. Rev. Lett.*, vol. 94, no. 12, 2005, Art. no. 123001.

[8] J. Li *et al.*, "SERF atomic magnetometer–recent advances and applications: A review," *IEEE Sensors J.*, vol. 18, no. 20, pp. 8198–8207, Oct. 15, 2018.

[9] S. J. Seltzer, "Developments in alkali-metal atomic magnetometry," Ph.D. dissertation, Dept. Phys., Princeton Univ., Princeton, NJ, USA, 2008.

[10] S. Cabrera *et al.*, "Structural analysis of the passive magnetic shield for the ITER heating neutral beam injector system," *Fusion Eng. Des.*, vols. 96–97, pp. 416–419, Oct. 2015.

[11] E. Calvo *et al.*, "Passive magnetic cylindrical shielding at gauss-range static fields," *Nucl. Instrum. Methods Phys. Res. A, Accel. Spectrom. Detect. Assoc. Equip.*, vol. 600, no. 3, pp. 560–567, Mar. 2009.

[12] C. P. Bidinosti and J. W. Martin, "Passive magnetic shielding in gradient fields," *AIP Adv.*, vol. 4, no. 4, 2014, Art. no. 047135.

[13] I. Moric *et al.*, "Magnetic shielding of the cold atom space clock PHARAO," *Acta Astronautica*, vol. 102, pp. 287–294, Sep./Oct. 2014.

[14] K. Tashiro, H. Wakiwaka, K. Matsumura, and K. Okano, "Desktop magnetic shielding system for the calibration of high-sensitivity magnetometers," *IEEE Trans. Magn.*, vol. 47, no. 10, pp. 4270–4273, Oct. 2011.

[15] T. W. Kornack, R. K. Ghosh, and M. V. Romalis, "Nuclear spin gyroscope based on an atomic comagnetometer," *Phys. Rev. Lett.*, vol. 95, no. 4, p. 230801, Nov. 2005.

[16] J. Li, W. Quan, B. Han, F. Liu, L. Xing, and G. Liu, "Multilayer cylindrical magnetic shield for SERF atomic co-magnetometer application," *IEEE Sensors J.*, vol. 19, no. 8, pp. 2916–2923, Apr. 15, 2019.

[17] F. Thiel, A. Schnabel, S. Knappe-Grüneberg, D. Stollfuß, and M. Burghoff, "Demagnetization of magnetically shielded rooms," *Rev. Sci. Instrum.*, vol. 78, no. 3, Feb. 2007, Art. no. 035106.

[18] J. Bork, H. Hahlbohm, R. Klein, and A. Schnabel, "The 8-layered magnetically shielded room of the ptb: Design and construction," in *Proc. 12th Int. Conf. Biomagnetism*. Espoo, Finland, 2001, pp. 970–973.

[19] D. Cohen, U. Schläpfer, S. Ahlfors, M. Hämäläinen, and E. Halgren, "New six-layer magnetically-shielded room for meg," in *Proc. 13th Int. Conf. Biomagnetism. Jena, Germany, VDE Verlag*, May 2002, pp. 919–921.

[20] G. Kajiwara, K. Harakawa, H. Ogata, and H. Kado, "High-performance magnetically shielded room," *IEEE Trans. Magn.*, vol. 32, no. 4, pp. 2582–2585, Jul. 1996.

[21] K. Harakawa, G. Kajiwara, K. Kazami, H. Ogata, and H. Kado, "Evaluation of a high-performance magnetically shielded room for biomagnetic measurement," *IEEE Trans. Magn.*, vol. 32, no. 6, pp. 5256–5260, Nov. 1996.

[22] T. W. Kornack, S. J. Smullin, S.-K. Lee, and M. V. Romalis, "A low-noise ferrite magnetic shield," *Appl. Phys. Lett.*, vol. 90, May 2007, Art. no. 223501.

[23] S.-K. Lee and M. V. Romalis, "Calculation of magnetic field noise from high-permeability magnetic shields and conducting objects with simple geometry," *J. Appl. Phys.*, vol. 103, no. 8, 2008, Art. no. 084904.

[24] E. Paperno, S. Peliwal, M. V. Romalis, and A. Plotkin, "Optimum shell separation for closed axial cylindrical magnetic shields," *J. Appl. Phys.*, vol. 97, no. 10, May 2005, Art. no. 10Q104.

[25] E. Burt and C. R. Ekstrom, "Optimal three-layer cylindrical magnetic shield sets for scientific applications," *Rev. Sci. Instrum.*, vol. 73, no. 7, pp. 2699–2704, 2002.

[26] E. Paperno, M. V. Romalis, and Y. Noam, "Optimization of five-shell axial magnetic shields having openings in the end-caps," *IEEE Trans. Magn.*, vol. 40, no. 4, pp. 2170–2172, Jul. 2004.

[27] S. Malkowski *et al.*, "Technique for high axial shielding factor performance of large-scale, thin, open-ended, cylindrical metglas magnetic shields," *Rev. Sci. Instrum.*, vol. 82, no. 7, Jul. 2011, Art. no. 075104.

[28] T. J. Sumner, J. M. Pendlebury, and K. F. Smith, "Convectional magnetic shielding," *J. Phys. D, Appl. Phys.*, vol. 20, no. 9, p. 1095, 1987.

[29] E. Paperno, H. Koide, and I. Sasada, "A new estimation of the axial shielding factors for multishell cylindrical shields," *J. Appl. Phys.*, vol. 87, no. 9, pp. 5959–5961, Apr. 2000.

[30] E. Paperno, I. Sasada, and K. Tashiro, "Experimental correction of the axial shielding equation," *IEEE Trans. Magn.*, vol. 38, no. 5, pp. 3324–3326, Sep. 2002.

Jundi Li received the M.S. degree from Beihang University, Beijing, China, in 2012, where she is currently pursuing the Ph.D. degree with the Innovative Research Institute of Frontier Science and Technology.

From 2012 to 2014, she was a Junior Engineer with the China Helicopter Design Institute, China. Her main research interests include the design of magnetic shield systems, inertial and magnetic measurements, and SERF atomic magnetometer.

Wei Quan received the Ph.D. degree in precision instruments and mechanics from Beihang University, China, in 2008.

He is currently a Professor with the Innovative Research Institute of Frontier Science and Technology, Beihang University. His current research interests include atomic spin inertial measurement, atomic magnetic field measurement, and information fusion navigation.

Bangcheng Han was born in February 1974. He received the M.S. degree from Jilin University, Changchun, China, in 2001, and the Ph.D. degree from the Changchun Institute of Optics, Fine Mechanics and Physics, Chinese Academy of Sciences, Changchun, in 2004.

In 2004, he was a Postdoctoral Research Fellow with the School of Instrumentation Science and Optoelectronics Engineering, Beihang University, Beijing, China. In 2006, he joined Beihang University, where he is currently a Professor with the Innovative Research Institute of Frontier Science and Technology. He is also with the Beijing Engineering Research Center of High-Speed Magnetically Suspended Motor Technology and Application, Beijing University of Aeronautics and Astronautics. He has more than 50 journal and conference publications. His research interests include mechatronics, magnetic suspension technology, and attitude control actuators of spacecrafts.

Zhuo Wang was born in Handan, China, in 1983. He received the B.E. degree in automation from Beihang University, Beijing, China, in 2006, and the Ph.D. degree in electrical and computer engineering from The University of Illinois at Chicago, Chicago, IL, USA, in 2013.

He was a Postdoctoral Fellow with the Department of Electrical and Computer Engineering, University of Alberta, from 2013 to 2014. He was a Research Assistant Professor with the Fok Ying Tung Graduate School, Hong Kong University of Science and Technology, from 2014 to 2015. He was selected for the 12th Recruitment Program for Young Professionals by the Organization Department of the CPC Central Committee and the 100 Talents Program by Beihang University, Beijing, China, in 2015. He is currently a Professor and a Ph.D. Instructor with the Innovative Research Institute of Frontier Science and Technology, Beihang University.

Dr. Wang is a member of the Adaptive Dynamic Programming and Reinforcement Learning Technical Committee, IEEE Computational Intelligence Society, the Data Driven Control, Learning and Optimization Professional Committee, CAA, and the Fault Diagnosis and Safety for Technical Processes Professional Committee, CAA. He is an Associate Editor of the IEEE TRANSACTIONS ON SYSTEMS, MAN, AND CYBERNETICS: SYSTEMS and *IET Control Theory & Applications*, and the *International Journal of Pattern Recognition and Artificial Intelligence*.

Jiancheng Fang was born in Shandong, China, in 1965. He received the B.S. degree in electrical engineering from the Shandong University of Technology, Jinan, China, in 1983, the M.S. degree in automotive engineering from Xian Jiaotong University, Xian, China, in 1988, and the Ph.D. degree in mechanical engineering from Southeast University, Nanjing, China, in 1996.

He is currently the Vice President of Beihang University, Beijing, China. He holds a special appointment professorship with the title of Cheung Kong Scholar, which was jointly established by the Ministry of Education of China and the Li Ka Shing Foundation. He has authored or coauthored over 150 articles and four books. His current research interests include the attitude control system technology of spacecraft, novel inertial instrument and equipment technology, inertial navigation, SERF atomic magnetometer, and co-magnetometer.